J. Condensed Matter Nucl. Sci. 25 (2017) 159–180

Research Article

Exothermic Reactions in the Partially Molten Li–Ni–Cu Alloy

Andras Kovacs*, David Brown and Fredrik Ek

Fiskarsin Voima oy, Nordanvik 142, 02580 Sjundeå, Finland

Abstract

Experiments with Li–Ni–Cu alloy, as a novel energy source, are described. The experiments are performed in the 1200–1300°C temperature range, using welded metallic containers and also in open tube under inert gas flow. The measured reaction energy is too high to be explained by chemical origin. The initial experiments elucidate the properties of this reaction, while the last experiment demonstrates its continuous operation.
 ISSN 2227-3123

Keywords: Continuous operation, High power rate, Lithium–nickel–copper fuel, Nuclear reaction, Temperature cycling

1. Introduction

An energy generating reaction arising within a metallic alloy has great potential utility. The aim of this study has been to investigate the possible reaction between Lithium and Nickel at elevated temperature. The theoretical possibility of $^{58}\mathrm{Ni} + 2\mathrm{e}^- \rightarrow {}^{58}\mathrm{Fe}$ double electron capture reaction, which liberates nearly 2 MeV energy, provides motivation to explore its practical realization, and we suspect Lithium to play a role in enabling such reaction. However, it is also known that having only a molten alloy of Lithium and Nickel is not yet sufficient for initiating an exothermic reaction [1]. We, instead, propose a Li–Ni–Cu system to initiate a reaction. The simplicity of the Li–Ni–Cu system is, in general, particularly useful for the development and validation of corresponding theoretical models, and the selected experimental setup is, in particular, relatively easy to reproduce and commercially scale.

2. Experimental Setup

The precursor metals were placed in a metallic container made of APM material (composition: 72% Fe, 22% Cr, 6% Al, m.p.: 1500°C, good oxidation resistance), and TIG-welded to ensure airtight sealing and significant overpressure tolerance even at high temperatures. The enclosed air volume was about 1 cm^3 per container in the initial four experiments. The employed furnace heated the sample from three directions, to achieve good temperature uniformity. The heating filaments were made of Kanthal wire (m.p. 1500°C, high oxidation resistance), having 1 mm diameter

*E-mail: andras.kovacs@broadbit.com

 ISSN 2227-3123

and 22 m length. S-type and N-type thermocouples were used for temperature sensing. The heating was controlled by temperature threshold triggered on/off switching in all cases, except the second and third experiments where thyristor electronics was used for precise heating power control. Figure 1 shows the reactor schematics.

3. Solid-state Li-Ni Alloying

An amount of 0.5 g Ni powder and 0.1 g Li was enclosed in the metallic container, and heat treated by being held for approximately 1 h at 1200°C. There was no excess heat detected during the heat treatment. After cooling and opening the container, an air-stable material was found inside, with metallic appearance. All the powders were sintered into a single solid. No free Li metal was observed. In summary, this experiment demonstrated that Li even up to 20 wt.% helps for the sintering of Ni powder, and diffuses well into the solid state metal.

4. First Experiment with the High Temperature Li–Ni–Cu Alloy

An amount of 2 g of Constantan wires (55% Cu + 45% Ni alloy, purchased from Conrad) and 0.06 g Li was loaded into a metallic container, and sealed by welding. Figure 2 shows the Cu–Ni alloy's phase diagram.

The sample was held at 1200°C, then the temperature was increased to 1300°C. After 10–15 min at 1300°C, an event occurred, which breached the metallic container wall (about 2 mm thick at thinnest part) and melted the heating wires above the sample, as well as the ceramic tube around which the wires are coiled. No detected sound accompanied this event. Figure 3 shows the damaged reactor and resulting appearance of the sample.

It can be observed in Fig. 3 that the container has bulged out along the drilled shaft (about 3/4 of the container length from the left), which indicates significant internal pressure and/or high temperature. While the originally enclosed O_2

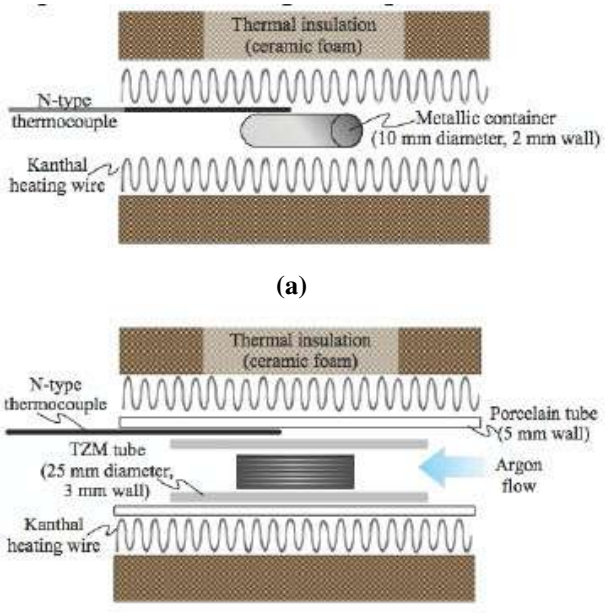

Figure 1. Reactor schematics for the container (*top*) and flow (*bottom*) experiment setups.

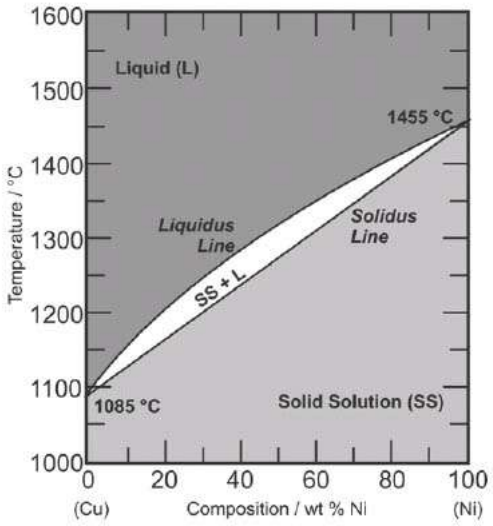

Figure 2. Cu–Ni phase diagram [2].

and N_2 gases react with molten Li already at the early phase of the heat treatment, Li_3N is known to decompose already below 1300°C. As the temperature approaches 1300°C, the estimated overpressure inside the container is 3 bar. Since the previously described Li–Ni alloying experiment showed no similar signs of bulging or container failure, some reaction process generated a higher internal pressure and/or a wall-softening higher internal temperature.

The leftover contents have the appearance of Ni_3O_4 and CuO material. Such thorough and complete burning of the sample indicates a significantly elevated temperature at the time of the container wall failure. The damage to the reactor material indicates that the ejected molten metal had a temperature well above 1500°C. This damage cannot be explained by Li vapor burning, because even a sideways flying molten metal droplet has melted the Kanthal wires, as can be seen on the upper tube in Fig. 3. Also, the complete breaching of the APM wall is consistent with a structural damage caused by very high internal temperature. Therefore, it appears that a sudden localized event has increased the internal temperature well above 1500°C in certain parts of the container, and then caused the ejection of molten metal. A gamma-ray detector showed no signs of radioactivity in the resulting sample.

5. Instrumented Observation of a Single Reaction Event in the Li–Ni–Cu Alloy

The molten Li–Ni–Cu alloy experiment was repeated with an improved setup, employing more precise computer control and temperature logging, and thicker walls of the APM container. Constantan wires of 2 g and 0.06 g of Li were again loaded into the metallic container. An N-type thermocouple was in direct contact with the container's outer wall for precise temperature logging.

Figure 4 shows the temperature logged during the experiment, from the point of exceeding 1200°C. The vertical axis shows the temperature and the horizontal axis shows the number of elapsed seconds from the start of heating. After reaching 1280°C, the heating program has been set to maintain a temperature of 1250°C. Approximately 1 kW of power was required to maintain the temperature of this reactor at 1250°C. An exothermic reaction apparently started at 1540 s, i.e. 9 min after exceeding 1200°C.

It can be seen in Fig. 4 that the control electronics gradually reduced the heating power as the temperature rose

(a)

(b)

(c)

Figure 3. View of the damaged reactor with breached container (a), zoom onto the melted part of the reactor (b), and the remainders of the container and sample material inside (c).

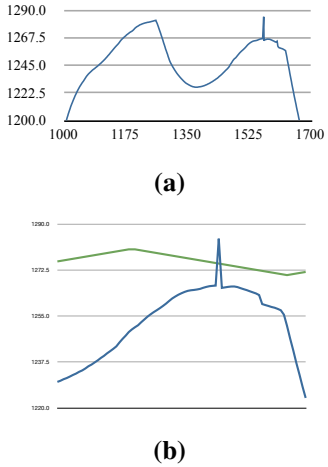

Figure 4. The temperature log of the experiment, with the green line showing heater voltage overlay (arbitrary scale.

above 1250°C. At about 1550 s time the thermocouple registered a sudden 20°C spike in temperature. We believe that this apparent spike is a signature of an X-ray emission burst, which was directly heating the thermocouple junction. The frequency of such radiative bursts is analyzed in more detail in a later section. Concurrently, a 'metal geyser' erupts from the container, once again melting through the heating filaments and ceramic tube above the container. Subsequently, all heating power is lost. As in the previous experiment, no sound was detected accompanying this event. Figure 6 shows the resulting view of the container after cooling. As detailed below, this reaction onset seems to be directly preceded by some melting of the Li–Ni–Cu alloy.

Note the observation of multiple similar upward spikes in subsequent experiments, such as shown in Fig. 12. The heating wires have not been broken in these follow-on experiments

Figure 5 shows details of the temperature history around the reaction event. The color coding of Fig. 5 shows our interpretation of the signal data. The yellow shading indicates either melting events or some other endothermic process inside the container, characterized by temporary slowing of the temperature rise. The radiative emission burst is a signature of the reaction event. Since the heating power is lost as a consequence of the reaction, the green shaded region indicates a temperature rise caused by the reaction itself. This interpretation is consistent with the effect of

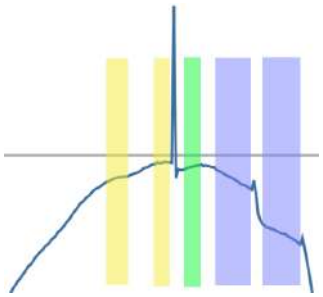

Figure 5. Temperature curve around the reaction event, the shading highlights the reaction related events.

spatial separation between the thermocouple (placed in the middle of the container) and the reaction hotspot (eruption is near the container end). A number of observations combine to indicate the localized hot-spot nature of the reaction:

- It was observed in the previous experiment that the ejected molten metal's temperature is above 1500°C, yet the thermocouple registers only a small temperature rise at the external container surface.
- While the radiative burst lasts for less than a second, the corresponding temperature rise is spread over several seconds and arrives with some delay, as the heat had to diffuse from the reaction site to the thermocouple to be detected.
- The small temperature rise registered at the top of container and a few centimeters from the molten metal burst location indicates a highly localized reaction hot-spot.

The radiative burst indicates the actual timing of the run-away reaction; there is a small subsequent local cooling due to lost heating power, followed by a gradual temperature rise from the propagated reaction heat, and finally followed by the cooling phase. In the cooling phase the slower cooling blue shaded regions indicate either the partial freezing of the container content or an ongoing exothermic process. Signatures of minor radiative bursts can be seen at the edge of the shaded regions.

After cooling, the container was opened. Its cross section is shown in Fig. 7. The 'metal geyser' apparently only transferred materials out of the container and then resealed itself, without any resulting hole in the container. Thus, apparently no external air entered the container. Consequently, Fig. 7 shows metallic surfaces across the container's interior, indicating that the exothermic reaction indeed happened within the Li–Ni–Cu alloy and was not due to oxidation with air. The melting of the ceramic tube and heating wires indicates that the internal reaction temperature was well above 1500°C at certain spots.

As can be seen in Fig. 7, a reddish shade appears at some spotty locations of the inner surface, while the bulk of the reaction material remains metallic gray. This indicates a copper accumulation on the metal surface, which might be caused by a segregation mechanism during solidification. It is also possible that an immiscibility gap appeared that was responsible for the separation of a Cu-rich liquid phase. The relationship between this behavior and the exothermic reaction is not clear at this stage but should deserve more investigation.

Figure 6. The container at the end of the experiment, with the view of the frozen metal geyser.

Figure 7. The cross-section view of the opened-up container, showing non-oxidized metallic surfaces along its interior.

A gamma-ray detector showed no signs of radioactivity in the resulting sample. Altogether, the above observations indicate that the observed reaction is of a localized run-away reaction type. To confirm this hypothesis, in subsequent experiments we expect to see radiative bursts of varying magnitude and temperature jumps of various magnitude/steepness. The spread of these quantities is expected to vary with the reaction-sensor distance and with the hot-spot reaction energy.

6. Exploring the Effect of Phase Change Events

A third molten Li–Ni–Cu alloy experiment was carried out with the following setup: the welded APM container was embedded into an approximately 0.5 cm thick ceramic encasement to prevent the spilling of bursting metal and to slow the thermal heating/cooling of the sample inside. Constantan wires of 4 g (Alfa Aesar) and 0.12 g Li were loaded into the metallic container. An N-type thermocouple was placed in direct contact with the ceramic encasement.

The temperature was raised in a stepwise fashion to different target temperatures, and at each target temperature to cycle $\pm 1^{\circ}$C around the target. This methodology allows precise detection of phase changes and radiative noise. Figure 8 shows the observed temperature plots.

The normal 'eventless' operation would be a smooth temperature cycling curve within the $\pm 1^{\circ}$C target tolerance limits. Every chart of Fig. 8 shows the time segment just after reaching the new target temperature from the previous lower temperature.

At every tested temperature, the temperature plot is initially a smooth cycle, then, after phase-change events, it becomes noisy for some minutes, and subsequently becomes smooth again. Based on the previous experiment, the observed noise is interpreted as the reaction's radiative noise signature. The noise amplitude is smaller in this test than in the previous one, which is in line with the thermocouple being further away from the sample due to the ceramic encasement. This observed pattern supports our previous assumption that the reaction takes place at the solid metal surface; i.e. the reaction spontaneously initiates whenever a fresh new solid surface is generated. It also points to the transient or self-limiting nature of the observed phenomenon; the reaction appears to last for 2–3 min only in each case.

The intensity of the observed events does not seem to depend on the temperature. Figure 9 shows the temperature plot at 1310°C, which is essentially eventless. At this temperature the Li–Ni–Cu alloy is assumed to be completely

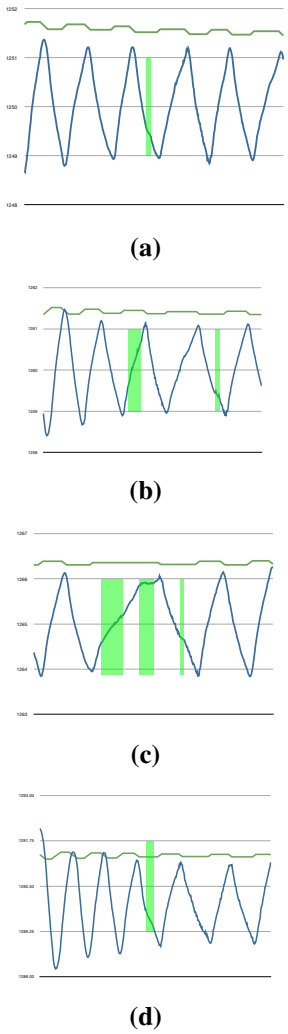

Figure 8. The temperature vs. time plot (*blue line*) at various reactor temperatures. The light green shading highlights either phase changes or some other endothermic/exothermic process. Each plot shows a 6–8 min time segment. The upper green curve shows the heater control voltage.

molten (Fig. 1). This observation supports our hypothesis that the reaction takes place at the surface of the solid phase and not in the molten phase.

After the conclusion of the experiment, it was noticed that some metal erupted from the container during the experiment, and flowed along the inner surface of the ceramic layer. The ceramic surface along the metal flow became shiny, indicating its local melting, which requires a temperature higher than 1500°C. The inside content of the APM container appears to have remained unexposed to air, as in the previous test.

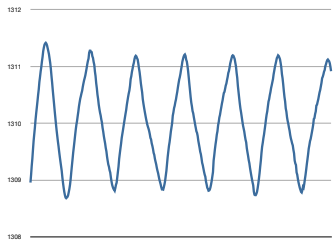

Figure 9. Temperature vs time plot at 1310°C (8 min segment).

7. Reaction Surface Cycling and Detection Of Reaction Heat Events

Since the observed reaction appears to terminate after a few minutes at a given temperature and since it appears to be triggered by a phase change, the question arises as to whether a stable reaction can be achieved through temperature cycling. The investigation of such temperature cycling was the aim of the fourth test. A further aim was to collect more heat signature data from the burst reaction events.

This experiment was carried out with the following setup: nine welded APM containers were embedded into an approximately 0.5 cm thick porcelain encasement. Constantan wires of 2 g and 0.06 g of Li were loaded into each container. As shown in Fig. 10, the N-type thermocouple was placed in the middle of the container cluster. The main purpose of the porcelain encasement in this improved setup was to ensure a uniform temperature of the containers. Since the thermocouple was embedded within this porcelain encasement, the measured temperature values in this setup correspond precisely to the container temperature at its given location. The containers are placed sideways from the heating wires, as there was not enough space to put them in the center.

After the experiment, some containers remained apparently un-breached while others breached. Figure 11 shows post-test views of some containers. In line with previous test observations, a bloating of the intact container can be observed and a dramatic damage on the breached container is observed. As the temperature control stayed below the Li boiling point throughout this experiment, and far below the APM melting point, this extensive container damage is an indication of the highly exothermic runaway nature of the observed reaction.

During this experiment the reactor temperature was cycled in an approximately ± 10°C range. Low level radiative bursts were persistent during this cycling experiment, demonstrating the feasibility of extending the reaction lifetime.

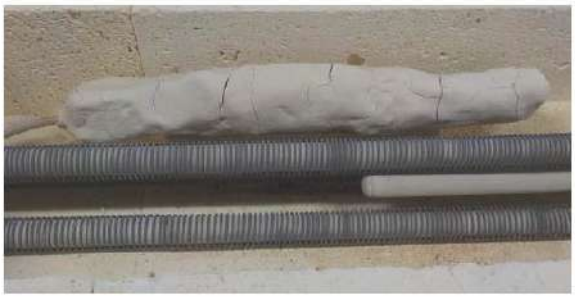

Figure 10. Photo of the container setup in this experiment. The N-type thermocouple is embedded under the porcelain encasement, and the S-type thermocouple measures the temperature between the heating spirals.

Figure 11. Post-test views of an apparently intact (slightly bloated) container and a completely breached container.

Figure 12 shows the temperature plot during one part of the temperature cycling process; the radiative bursts are seen to become periodically weaker and stronger during the cycling. This data confirms the few-minute lasting self-limiting reaction events, which were similarly observed in the previous experiment, and gives further evidence to the idea that the reaction takes place on the solid alloy surface. Based on this data, it is proposed that the reaction can be nearly continuous when temperature cycling has periodicity on the order of minutes. With slower temperature cycling periodicity, e.g. on the order of an hour, the reaction would be expected to persist for only a small fraction of the time.

The most notable direct reaction heat events are shown in Fig. 13. As expected, all events showed an abrupt temperature jump. The strongest one is in the first example, showing a 10°C jump followed by cooling towards the preceding temperature. This data indicates the reaction takes place through run-away events in strongly localized hot-spots.

The second example in Fig. 13 shows that the initial reaction heat event was detected already slightly below 1200°C, when there was no molten phase yet, indicating a minimum temperature for this reaction at the solid alloy surface.

Since more temperature jumps were observed than the number of breached containers (Fig. 13 shows only the most pronounced ones), and since similar temperature jumps were observed also in a later experiment under Ar-flow (e.g. the green curve of Fig. 17 shows a 6°C jump at 60 s time), these temperature jumps cannot be explained as sudden oxidation events.

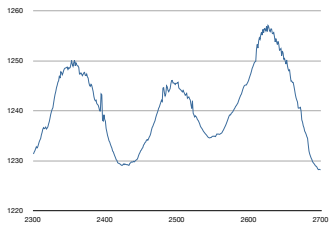

Figure 12. Temperature log of the temperature cycling process. The horizontal axis indicates the experiment time (seconds).

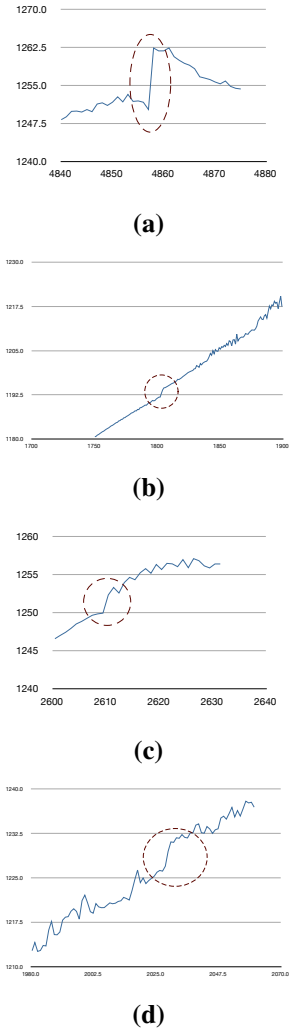

Figure 13. Highlights of the most pronounced temperature jump events. The horizontal axis indicates the experiment time (seconds).

Figure 14 shows the post-mortem metallic surfaces of the Li–Ni–Cu alloy. The round objects are ejected alloy metal pieces originating from some of the containers. The previously noted copper accumulation is even more clearly seen on these surfaces. As the copper concentration grows, the surface takes on a yellowish color, and then becomes copper-red in the spots where the copper is highly concentrated.

8. Peak Reaction Power Measurement

A fifth molten Li–Ni–Cu alloy experiment was carried out with an Ar-flow based setup: 15 g Constantan foils (Schlenk) and 0.5 g Li wires were loaded into an open TZM (99.4% Mo, 0.5% Ti, 0.1% Zr) metal tube. The TZM tube was placed

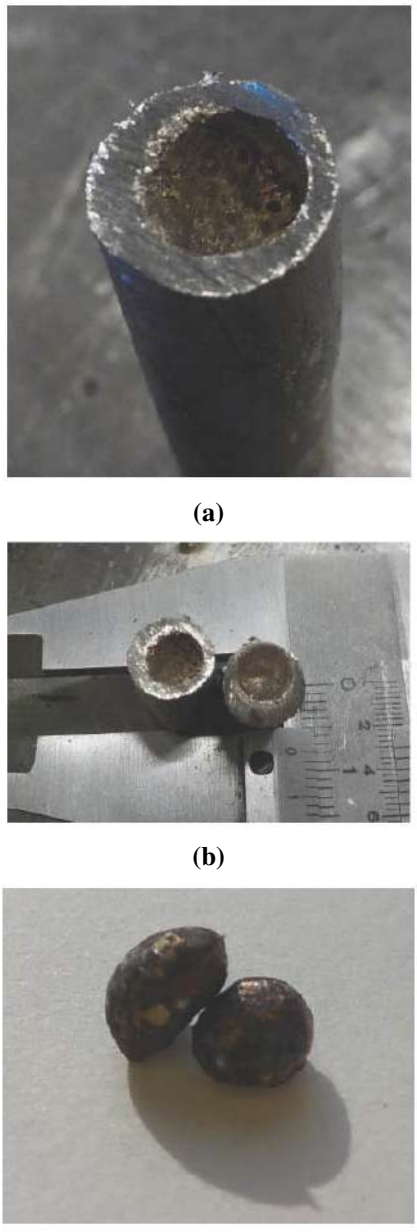

(a)

(b)

(c)

Figure 14. Apparent copper accumulation on the surfaces of the samples.

into a ceramic tube flooded with an Ar flow. An N-type thermocouple was placed between the TZM and ceramic tubes. The heating voltage and current were measured by a Voltcraft EL 4000 device.

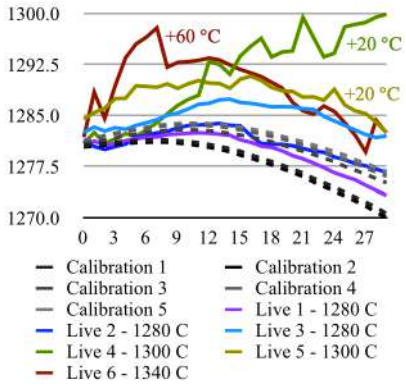

Figure 15. Post-heating temperature charts, showing 30 s evolution after heating stop.

This experiment was aimed at quantifying the reaction power and validating heat production. A calibration test was performed on the empty reactor, using the following temperature cycling program: constant power heating was used from 1200 to 1280°C, heating was turned off at the 1280°C upper temperature threshold, and then constant power heating was turned back on at the 1200°C lower temperature threshold. The employed heating power was approximately 1.5 kW. The dashed lines of Fig. 15 show 30 second segments of temperature evolution, starting from the moment when heating was turned off. The cooling rate was slightly decreasing in subsequent cycles as the insulating outer reactor walls heated up.

The live test run was started from the same room temperature initial condition as the calibration run, and upon reaching 1200°C the initial three cycles used the same heating program cycling between 1200°C and 1280°C thresholds. The purple-blue lines of Fig. 15 show the temperature evolution in these initial cycles, starting from the moment when heating was turned off. The shape and trend of these curves gradually diverges from corresponding calibration curves, indicating a start-up of the reaction. An exothermic reaction signature is noticeable in each temperature cycle.

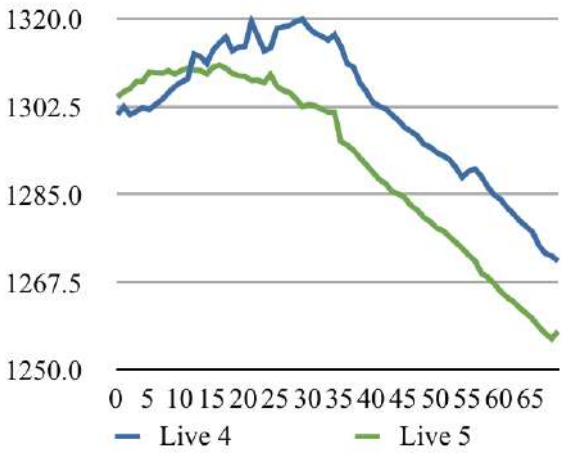

Figure 16. Comparison of live run's cycle 4 vs. 5 cooling phase temperature charts, showing 70 s duration post-heating segment.

In the third cycle, the temperature was rising for 14 s after turning off the heating, and stayed above 1280°C even 30 s after turning off the heating.

In the next two temperature cycles the upper threshold limit was adjusted to 1300°C. For the sake of comparison, Fig. 15 shows the corresponding temperature evolution (green curves) with a –20°C offset. It is noted that while Figs. 8 and 9 show the container in almost thermal equilibrium, Fig. 15 shows the temperature evolution just after a heating rate of 20°C/min. The strongest self-heating event has been observed in cycle 4; it is therefore used for the peak power rate estimation. The repeated cycle at 1300°C showed much smaller self-heating power, essentially maintaining temperature for over 30 s. Finally, the last cycle, where heating remained turned on up to the 1340°C temperature threshold, showed very fast initial self-heating which extinguished after 7 s. This is consistent with the eventless over-1300°C behavior shown in Fig. 9.

To estimate the peak power rate, Fig. 16 compares cycle 4 to cycle 5 cooling just after the heating was switched off. As a conservative estimate, we neglect any reaction heat which cycle 5 has produced during this time. The exothermic reaction of cycle 4 caused self-heating within the 6–26 s time segment, i.e. about 20 s duration. The subsequent time-wise separation of the cooling curves was 13 s. Considering that the 1.5 kW heating was turned on 69% of the time during calibration, it took 1 kW average heating power to maintain the reactor temperature. Therefore self-heating rate of cycle 4 shown in Fig. 15 was at least 650 W, in order to have generated the 13 s time-wise separation[a]. This corresponds to a peak power rate of 42 W/g with respect to the mass of reaction materials.

A longer time view of the temperature evolution is shown in Fig. 17, where the vertical line indicates the time when the electric heating was turned off. This figure uses same color coding as Fig. 15, but without any temperature offsets.

It is seen also from Fig. 17 that while all calibration temperature curves are very smooth, the live test runs are increasingly erratic. The first two calibration runs have significantly lower slope than the other calibrations or the first two live runs. Their lower slope might have been caused by some transitory effect relating to the warm-up or initial usage of this flow reactor.

Energy-producing time periods can be visually gauged as those segments where the slope of temperature change significantly deviates from the calibration slopes. Qualitatively, the most noteworthy heat-producing time periods are:

- 120–150 s of cycle 4; pure self-heating causes continuous temperature rise,
- 0–120 s of cycle 5; rise gradient was noticeably higher than during calibration,
- 72–130 s of cycle 6; rise gradient had an inflection point and transitioned to higher value.

In summary, the exothermic reaction was observed to produce heat at a peak rate of 42 W/g with respect to the mass of reaction materials; this power rate lasted for 20 s. With the above-described temperature cycling program, several heat-producing time periods were observed during the 40 min experiment run.

Considering all the previous experimental observations, we propose that the exothermic reaction raises the reaction hot-spots' temperature well above the Li boiling point. The evaporating Li causes a significant pressure rise, and the bulging and bursting of the APM containers. In this experiment run, we observed that the evaporated Li was evacuated from the reactor by the Ar flow. Figure 18 shows the blackened inner surface of the ceramic tube downstream, onto which Li condensed out. No discoloration of the tube was observed upstream. This hypothesis implies that the observed exothermic reaction might be sustained for a longer time with the combined use of temperature cycling and a leak-free container.

Figure 19 shows the post-experiment view of the reaction tube. Parts of the metal foils retained their original shape, parts were melted around the tube walls, and parts clumped together, e.g. the piece seen in the middle of the image. The de-alloying of copper is again clearly observable along the walls. Although the metals were not physically

[a]That is 13 × 1000/20 W.

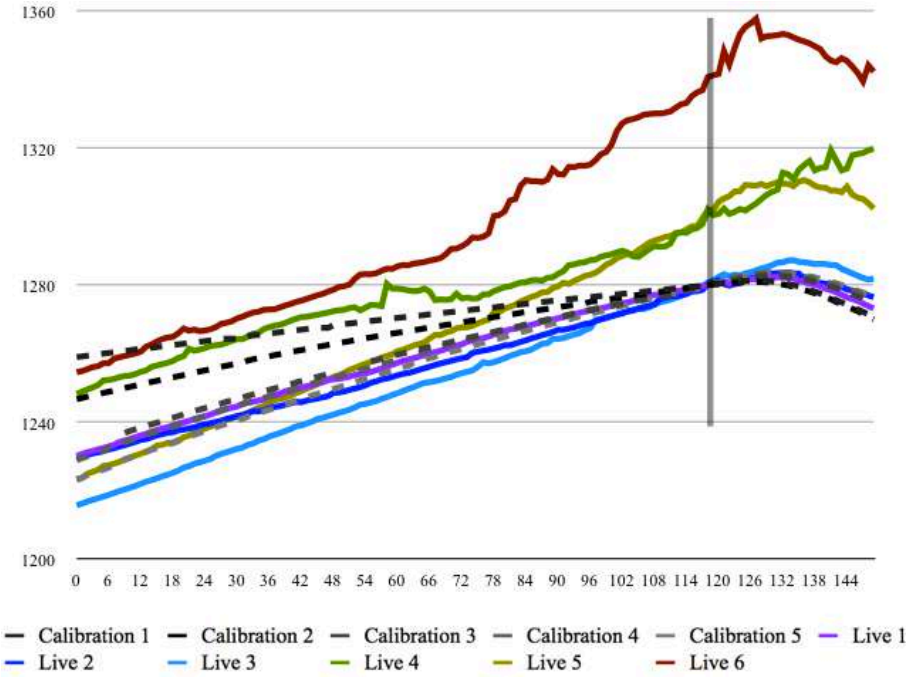

Figure 17. Temperature evolution during the last 2 min of heating, and the sub-sequent 30 s without external heating.

confined in the tube, they did not flow out because the tube has been sufficiently long to retain the molten metals inside, as seen in Fig. 19.

9. Average Reaction Power Measurement

A sixth molten Li–Ni–Cu alloy experiment was carried out with a N_2-flow based setup: 9.52 g Constantan foils (Schlenk) and 0.28 g Li pieces were loaded into a steel tube, and sealed by welding. This steel container was then

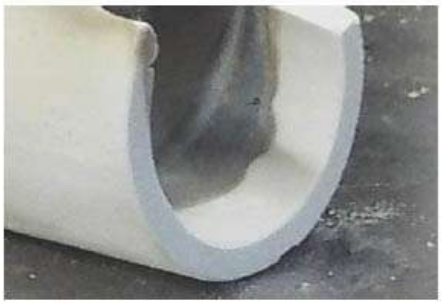

Figure 18. Post-experiment view of the downstream ceramic tube surface.

Figure 19. Post-experiment view of the reaction materials inside the TZM tube.

placed into a TZM (99.4% Mo, 0.5% Ti, 0.1% Zr) metal tube, and sealed by welding. The schematics of this reactor setup is shown in Fig. 20.

This choice of container materials was motivated by the consideration of Li alloying/corrosion issues. While Li is known to be corrosive to most metals [3–5], especially at high temperatures, the employed container must be inert with respect to molten Li. Fe and Mo are suitable materials for containing high temperature molten Li, and most importantly Mo has a high melting point of 2600°C. By welding the TZM container, we have achieved a container with both high strength and high melting point, which is suitable for long term testing. The reactor was equipped with two thermocouples; the first one above the TZM container, and the second one approximately above the N_2-flow inlet. The N_2 sheath flow exited the reactor through small fissures at the top of the reactor chamber. The first thermocouple was used for the heating control feedback. Consequent to the above-described reactor structure, during the experiment the temperature at the second thermocouple was somewhat lower than the temperature at the first one.

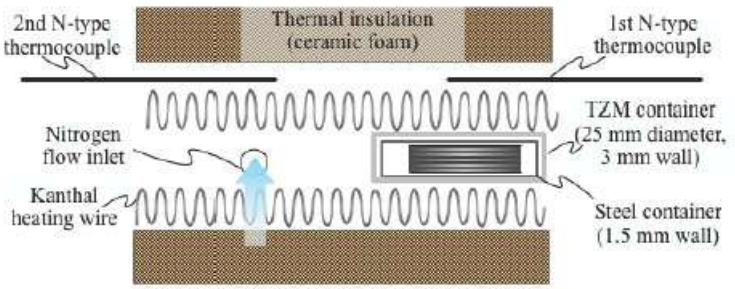

Figure 20. Reactor schematics for the TZM container based experiment setup.

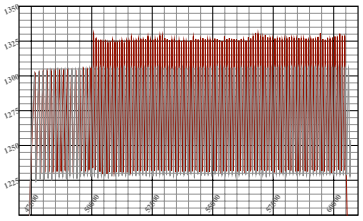

Figure 21. Temperature evolution of the first thermocouple during calibration (*gray*) and live experiment run (*red*).

A calibration run was first performed for measuring the baseline power consumption, followed by the live experiment run. Both runs used the same temperature program, the only difference was the absence of the TZM container in the calibration run. The temperature program consisted of ramping up the reactor temperature to its operational range over 13 h, followed by the temperature cycling program: constant power heating was used from 1240 to 1300°C, the heating was turned off at the 1300°C upper temperature threshold, and then the constant power heating was turned back on at the 1240°C lower temperature threshold. The employed heating power was approximately 1.2 kW.

The goal of this experiment run was to perform average reaction power measurement over an extended time period. The thermocouples were Kanthal sheathed for continuous operation in this high temperature range. The previously performed peak power measurement, radiative emission detection, or heat burst detection were not in the scope of this experiment; the thicker container walls and the employed thermocouple sheathing allow only averaged reaction power measurement.

Figure 21 shows the comparative temperature evolution of the first thermocouple during calibration (gray curve) and live run (red curve). The vertical axis shows the temperature, and the horizontal axis shows the number of seconds since the start of the temperature program. The 47 500 s value corresponds to the starting time of temperature cycling in the 1240–1300°C operating range. The very similar initial periodicity of the two curves indicates that the heating and cooling powers are nearly the same at the start. The 60 500 s value corresponds to the breaking of the heating wire during the live run; the subsequent drop in temperature is seen at the right. We believe this wire failure was caused by the wire temperature being too close to its melting point near the end of heating cycles.

It can be seen in Fig. 21 that the calibration run proceeded as expected through this time window. During the initial half hour, the temperature evolution of the live run corresponded closely to the temperature evolution during the calibration. About 30 min into the temperature cycling, the abrupt rise of the maximum live temperature to 1325°C indicated the start-up of the exothermic reaction. Over the subsequent three hours, the very consistent temperature peak values indicated the continuous operation of this reaction. Such continuous operation and good controllability are essential for any industrial applicability of this new energy source.

Figure 22 shows the comparative temperature evolution of the first thermocouple (red curve) and second thermocouple (blue curve) during the live run. The vertical axis shows the temperature, and the horizontal axis shows the number of seconds since the start of the temperature program.

Initially, the temperature at the second thermocouple cycled in the 1185–1270°C temperature range. As discussed above, this lower temperature range is caused by the N_2-flow cooling effect. At the same time when the starting-up exothermic reaction caused a temperature rise at the first thermocouple, the second thermocouple showed a remarkable drop in its temperature range. This range shift was the consequence of its sensitivity to the reduced electric heating. The produced reaction heat caused the first thermocouple to reach the shut-off temperature threshold faster and to reach the next turn-on temperature threshold later, which reduced the ratio of time when the electric heating was on. As the second thermocouple was closer to the heating wires than to the TZM container, and since it was cooled to a

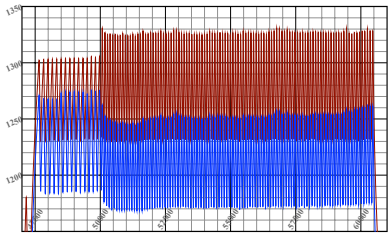

Figure 22. Temperature evolution of the first (*red*) and second (*blue*) thermocouple during the live experiment run.

larger extent by the N_2-flow, the net result was a temperature range downshift at this location. Altogether, the data of Figs. 21 and 22 are very consistent with the hypothesis of continuous energy production during the last three hours of the live experiment run.

Quantitatively, the average reaction power was measured from the time ratio of electric heating-on times, summarized in Table 1. During the initial half-hour of the temperature cycling, the calibration and live run heating-on time ratios are very similar. The average grid voltage during calibration is 234 V, while the average grid voltage during live run is 232 V; i.e. the electric heating power is 1.7% higher during calibration. Altogether, the electric power input is measured to be 5% higher during calibration. At least part of this power mismatch may be caused by some initial bursts of the exothermic reaction.

During the last three hours of the experiment, the mismatch between the heating-on time ratios was 0.25. This means that the reaction power was equivalent to having electric heating on 25% of the time. Since the electric heating power was 1.2 kW, the average reaction power was 300 W. This corresponds to 30 W/g average reaction power with respect to the fuel mass.

The cumulative reaction energy over these last three hours was over 3 MJ. This amount of reaction energy is larger than any possible chemical reaction. The airtight TZM container has remained intact by the end of the experiment run.

10. Radiation Analysis

The objective of the next experiment is to analyze the radiation emitted during the exothermic reaction. The same experimental setup was used as in the previous experiment, except that a flow of Ar was used instead of a flow of N_2. The low end of the emitted radiation spectrum was monitored by an oscilloscope capable of up to 10 MHz spectroscopy. The high end of the emitted radiation spectrum was monitored by a Geiger counter, which was placed about 40 cm from the fuel container.

To get a clear reaction signal, a simple heating program was used, to trigger a single runaway reaction event. The temperature evolution of the experiment is shown in Fig. 23. After thermal reactor stabilization at about 1260°C, constant-power heating was started, using about 1.2 kW heating power. This heating was maintained until the heating wire was broken by the intense heat. This event is indicated by the dashed line in Fig. 23 at ∼255 s. The horizontal axis shows the number of seconds from the start of constant-power heating. The onset of the reaction event is clearly

Table 1. Ratio of electric heating ON times

	Calibration	Live run
47 800– 49 800 s	0.63	0.61
50 200–60 200 s	0.58	0.33

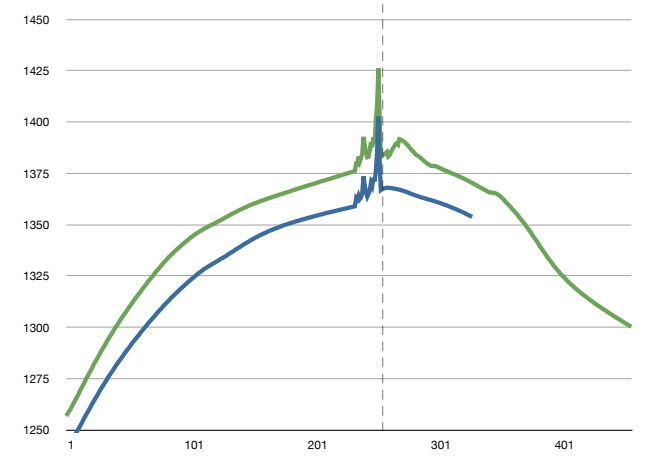

(a)

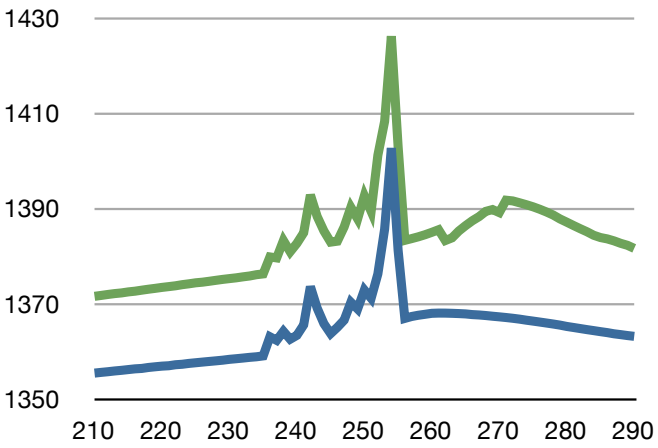

(b)

Figure 23. Temperature evolution measured by the first (*blue*) and second (*green*) thermocouple. The dashed line indicates loss of heating due to wire breaking.

seen in Fig. 23 at ∼235 s, and it is also noticeable that the reaction hotspot was close to the second thermocouple because only this thermocouple detects the continued temperature rise after heating stops.

The Geiger counter indicated an elevated radiation level for only 4–5 s duration, approximately coinciding with the largest peak seen in Fig. 23. The counting level was normal before and after this brief event. During this elevated

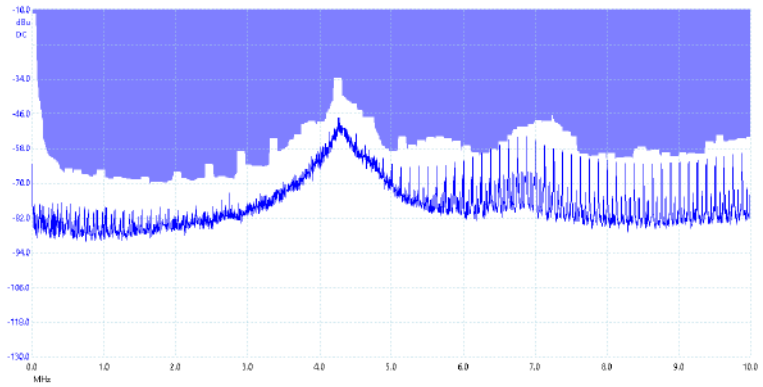

Figure 24. The background RF spectrum.

Geiger counter reading, a buzzing sound was heard from the reactor, similar to the sound of electric arcing.

The 235–255 s time segment of the thermocouple signal in Fig. 23 shows synchronized peaks between the two thermocouples, indicating radiative signal detection. Since the peaks are always in the positive direction only, and since the largest peaks have a measurable upwards and downwards slope, this signal is interpreted not as noise caused by an RF signal, but as radiative heating of the thermocouple junction. As discussed above, the reaction spot is close to the second thermocouple, and yet both thermocouples measure radiative heating peaks to have approximately the same magnitude. This observation indicates that the detected radiation frequency is strongly scattered by the metallic container; since both thermocouples are placed at equal distances from the metallic container, they detect scattered signals having approximately equal magnitude. Altogether, this thermocouple data indicates the radiative emission of X-rays. The frequency of detectable X-rays is constrained by the following requirements: high enough frequency to partially escape the metallic container, strong scattering by the metallic container, and strong enough interaction with the thermocouple junction to cause local heating of the thermocouple.

According to the minute-by-minute Geiger counter record shown in Table 2, an excess of 84 counts was produced over the 30 background counts during that reaction minute. As this excess count was concentrated in 4–5 s, it indicates about 40 times stronger radioactivity than the background signal.

Figure 24 shows the background RF spectrum measured before the experiment. The apparent peak near 4.2 MHz is caused by the increased sensitivity of the antenna geometry around that frequency; i.e., it is not a physical signal. The shaded region is the mask definition for log capture.

Figure 25 shows consecutive snapshots of RF spectrum captured during the reaction. The produced RF signal is approximately 20 dB above the background and is equally spread over the 1–10 MHz frequency range, which cannot

Table 2. One-minute resolution Geiger statistics relative to the reaction time.

	–5	–4	–3	–2	–1	0	1	2	3	4	5
Hits	31	33	17	40	31	114	34	34	23	29	33

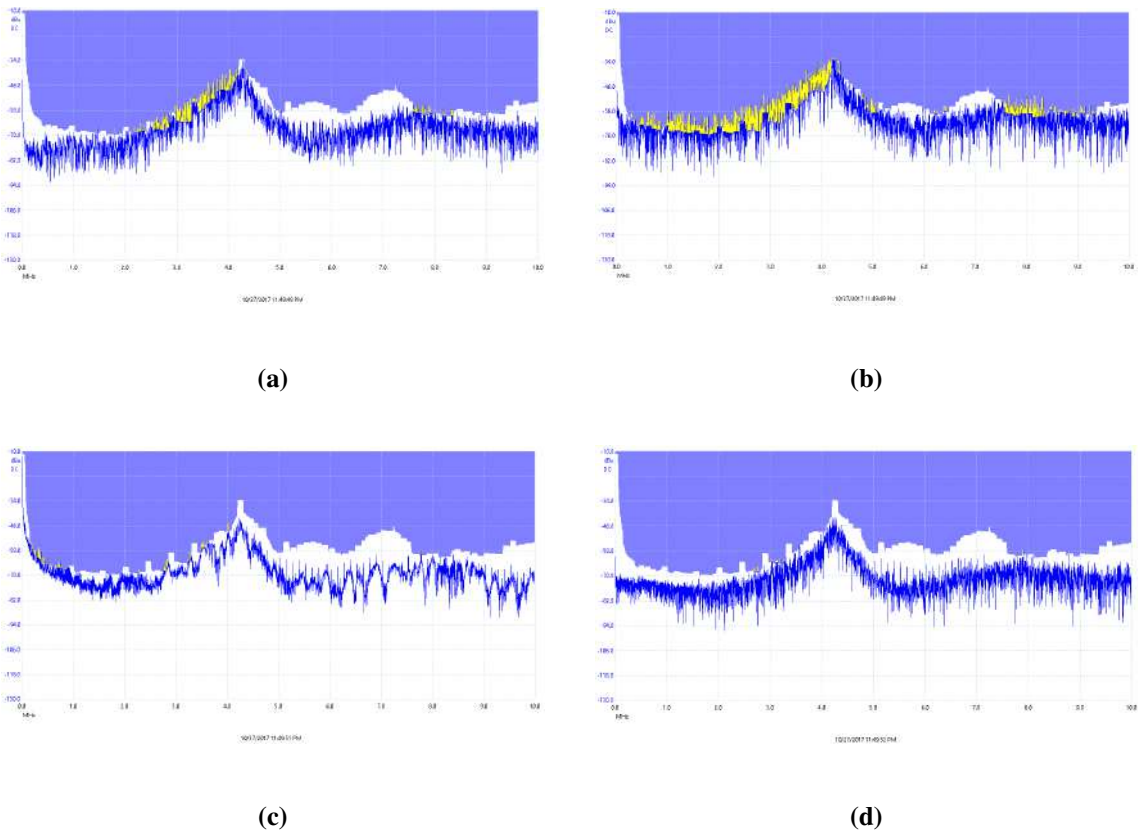

Figure 25. The RF spectrum evolution during the reaction event.

be produced by a chemical reaction or by arcing at the employed voltage. The consecutive snapshots show the rise and fading of this signal.

The third snapshot shows a stronger low-frequency component of the signal. This low-frequency component's shape and frequency range are characteristic of RF emission from electric arcing discharge. Therefore, this component is interpreted to be the signature of the electric arcing between the wires, whose presence was also detected from its sound. Since this signal is generated by ionized argon, it is not coming from the reaction itself; it is however an additional indicator of ionizing radiation.

Altogether, this electromagnetic emission analysis indicates a broad spectrum radiative emission spanning the RF, X-ray, and gamma frequency ranges. This data provides insights into the reaction signature and dynamics.

11. Conclusions

An exothermic reaction has been found to be spontaneously initiated in the Li–Ni–Cu alloy in the 1200–1300°C temperature range. The reaction is fully reproducible, with a 100% reproduction rate over the course of six test events. The reaction appears to be a series of localized run-away bursts at the Li–Ni–Cu alloy's solid surface, and is accompanied

by simultaneous broad spectrum radiative emission. The reaction self-extinguishes after a few minutes at constant temperature, but can be restarted via molten-solid phase cycling of the alloy surface. With a temperature cycling program, we have been able to sustain the reaction for about 3 h. The reaction is likely to be extendable to longer time scales. The average reaction power was approximately 30 W/g, while the peak power rate was approximately 40 W/g. With such power levels, this newly discovered reaction is industrially relevant. The described experimental setup facilitates further study and elucidation of the nature of this reaction. The planned scope of further experiments includes achieving longer experiment runs, and post-experiment isotope analysis of the reaction fuel.

Acknowledgements

The authors are grateful to Dr. Pekka Janhunen for the insightful consultation and advising, and to Pertti Heikkinen for the TZM material welding.

References

[1] US patent 3383204.
[2] http://www.spaceflight.esa.int/impress/text/education/Solidification/Phase_Diagrams.html.
[3] W.D. Manly, *Fundamentals of Liquid Metal Corrosion*, Oak Ridge National Laboratory, 1956.
[4] E.E. Hoffman and W.D. Manly, *Corrosion Resistance of Metals and Alloys to Sodium and Lithium*, Oak Ridge National Laboratory, 1957.
[5] G. DeVries, The corrosion of metals by molten lithium, in J.E. Draley and J.R. Weeks (Eds.), *Corrosion by Liquid Metals*, Springer, Boston, MA, 1970.